Data and Model-Driven Decision Support for Environmental Management of a Chromium Plume at Los Alamos National Laboratory – 13264

Velimir V. Vesselinov[*], Danny Katzman[**], David Broxton[*], Kay Birdsell[*], Steven Reneau[*], David Vaniman[***], Pat Longmire[***], June Fabryka-Martin[***], Jeff Heikoop[***], Mei Ding[***], Don Hickmott[***], Elaine Jacobs[***], Tim Goering[**], Dylan Harp[*], Phoolendra Mishra[*]

[*] Computational Earth Science (EES-16), Earth and Environmental Sciences, Los Alamos National Laboratory, Los Alamos NM 87545, U.S.A, vvv@lanl.gov

[**] Environmental Programs (ADEP), Los Alamos National Laboratory, Los Alamos NM 87545, U.S.A.

[***] Earth Systems Observations (EES-14), Earth and Environmental Sciences, Los Alamos National Laboratory, Los Alamos NM 87545, U.S.A

ABSTRACT

A series of site investigations and decision-support analyses have been performed related to a chromium plume in the regional aquifer beneath the Los Alamos National Laboratory (LANL). Based on the collected data and site information, alternative conceptual and numerical models representing governing subsurface processes with different complexity and resolution have been developed. The current conceptual model is supported by multiple lines of evidence based on comprehensive analyses of the available data and modeling results. The model is applied for decision-support analyses related to estimation of contaminant-arrival locations and chromium mass flux reaching the regional aquifer, and to optimization of a site monitoring-well network. Plume characterization is a challenging and nonunique problem because multiple models and contamination scenarios are consistent with the site data and conceptual knowledge. To solve this complex problem, an advanced methodology based on model calibration and uncertainty quantification has been developed within the computational framework MADS (http://mads.lanl.gov). This work implements high-performance computing and novel, efficient and robust model analysis techniques for optimization and uncertainty quantification (ABAGUS, Squads, multi-try (multi-start) techniques), which allow for solving problems with large degrees of freedom.

INTRODUCTION

A crucial aspect of any decision-making process for environmental management of contaminated sites is the development of scientifically defensible remediation strategies. Evaluation of specific remedial actions in terms of both their environmental benefits and cost effectiveness requires a robust conceptual model of the site and systematic characterization of conceptual model elements related to processes governing contaminant migration in the subsurface. Conceptual model uncertainties can be estimated based on detailed analyses of the available qualitative and quantitative site knowledge. The decision process also identifies potential data and conceptual-understanding gaps requiring additional data acquisition to refine remedy selection. The decision-making process is facilitated by implementation of robust computational techniques for decision support that take into account existing site uncertainties. However, due to data and knowledge gaps as well as complex interdependencies between uncertainties (conceptual elements, model parameters, measurement/computational errors, etc.), the decision-support optimization problem is typically non-unique, and the model-prediction uncertainties are frequently difficult to quantify. The problem is non-unique because multiple solutions produce reasonable agreement with the site data. [1-3]

We have performed detailed investigation of site information related to a chromium plume in groundwater beneath Los Alamos National Laboratory (LANL). The work includes hydrogeological, geophysical, mineralogic, petrographic, and geochemical studies for characterization of processes and asso-

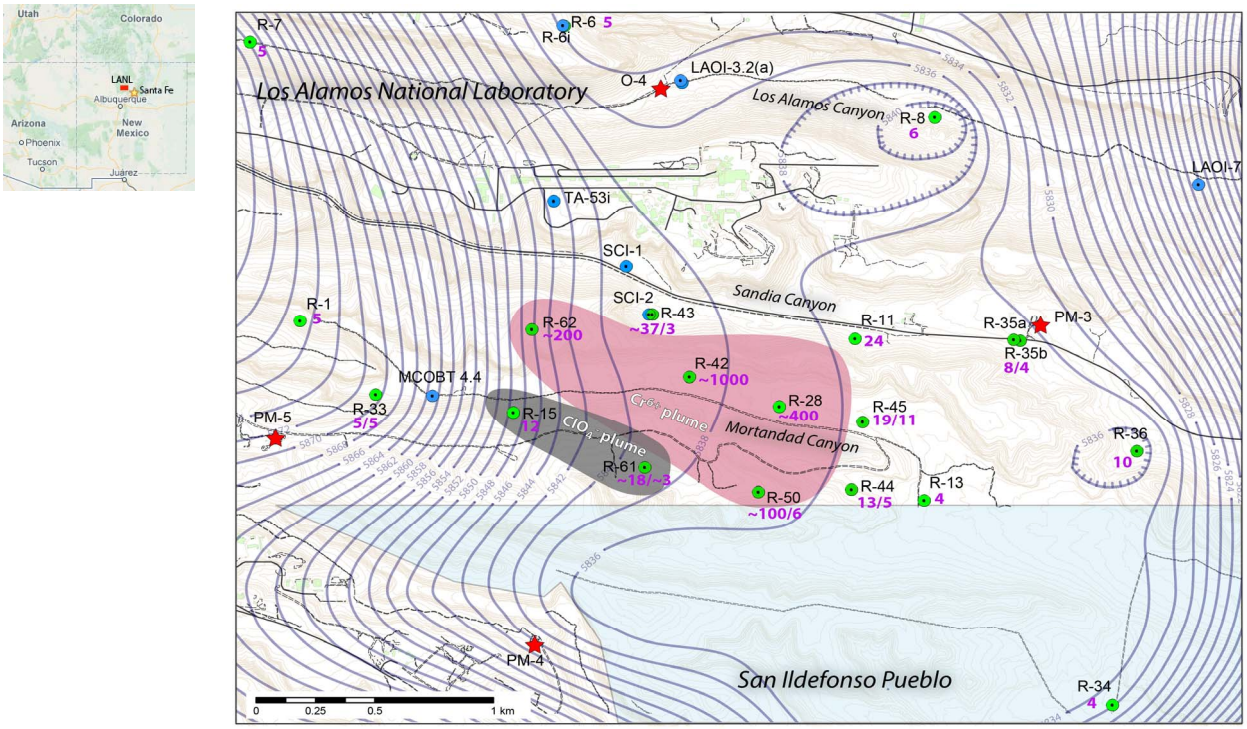

Figure 1: Location of the study site. Green and blue dots show the locations of aquifer and vadose zone monitoring wells, respectively. Red stars are municipal water supply wells. Recently observed Cr^{6+} concentrations (circa 2012) at each regional well are shown in purple [µg/ℓ]; the concentrations at two-screen wells (e.g. R-61) are shown as upper / lower screen values. The Cr^{6+} plume represents an area where concentrations are higher than 50 µg/ℓ (ppb). The ClO_4^- plume represents an area where elevated ClO_4^- concentrations exceed 4 µg/ℓ (ClO_4^- values are not shown). The blue contour lines represent the elevation of the regional water table (circa 2012) [ft]. Note: the wetland is outside the map area; it is 4.5 km northwest of R-62 along Sandia Canyon.

ciated parameters controlling groundwater flow and contaminant transport in the subsurface. Based on these data, we have developed a series of alternative conceptual and numerical models representing governing subsurface processes with different complexity and resolution. The current conceptual model is supported by multiple lines of evidence based on a series of comprehensive analyses of the data. The text below describes the site, the conceptual model of processes governing subsurface groundwater flow and contaminant transport, applied methodologies for simulation of subsurface processes, and analyses of modeling results related to decision making.

SITE DESCRIPTION

LANL is a research facility operated by the U.S. Department of Energy (DOE). The laboratory is in north-central New Mexico, and consists of a 103 km^2 area, mostly on the Pajarito Plateau, which is a series of mesas separated by eastward-draining canyons (Fig.1). LANL is currently investigating sites potentially contaminated by past operations to ensure contaminants do not threaten human health or the environment. The investigations are subject to the Compliance Order on Consent between the State of New Mexico Environment Department (NMED) and DOE [4].

One of the LANL contamination sites is related to a chromium (Cr^{6+}) plume in the regional aquifer beneath Sandia and Mortandad Canyons (Fig.1). A comprehensive investigation of this plume has been ongoing since 2005 [5-8]. The Cr^{6+} contamination results from infiltration of liquid effluents released from a power plant that provided electric power for LANL. The contaminated effluents were discharged in

Sandia Canyon between 1956 and 1972, when treated sanitary wastewater was used for power-plant cooling; the water was treated with potassium dichromate ($K_2Cr_2O_7$), phosphate, zinc, and sulfuric acid. The total Cr^{6+} mass release into the Sandia Canyon is estimated at 54,000 kg with uncertainty bounds between 31,000 to 72,000 kg. During that period, the water flux released in the canyon was about 500 to 1000 m^3/d; similar effluent volumes were probably discharged through 1992. The Sandia Canyon effluent also had elevated tritium (^3H) concentrations; in 1976-77, monthly measurement of ^3H concentrations ranged between 4200 pCi/ℓ and 38,500 pCi/ℓ [9]. Since the Cr^{6+} releases ceased in 1972, municipal water was used for cooling at the power plant, and chlorine, bromine, sodium molybdate, zinc chloride, other inorganic salts, and acrylate polymers have been applied as cooling water additives. In 1992, LANL consolidated its sanitary waste treatment to a single facility that discharges to Sandia Canyon. Since then, the released effluent in Sandia Canyon has been 1000 to 1500 m^3/d. In the next few years, Sandia Canyon effluent volume will be decreased to an estimated 200 to 400 m^3/d as part of LANL's Sanitary Effluent Reclamation Facility (SERF) project [8] which will reduce infiltration recharge along the canyon.

Cr^{6+} migration in the subsurface is also influenced by effluent discharges in two neighboring canyons: Mortandad and Los Alamos (Fig.1,2). Since 1963, LANL's Radioactive Liquid Waste Treatment Facility has discharged treated wastewater to Mortandad Canyon. Perchlorate (ClO_4^-), nitrate (NO_3^-), 1,4 dioxane ($C_4H_8O_2$), and tritium (^3H) released in Mortandad Canyon are detected in perched-intermediate zones. Some of these contaminants are partially collocated with Cr^{6+} released in Sandia Canyon and detected in the regional aquifer. The Mortandad releases have historical volumes about 10 times less than the Sandia releases; they averaged between 100 to 160 m^3/d during the 1960's through 1980 and have declined steadily since 1980. Between 2007 and 2010, the Mortandad Canyon releases averaged less than 20 m^3/d. Since August 2010, Mortandad Canyon discharges have effectively stopped. Past effluent releases in Los Alamos Canyon are characterized by elevated ^3H concentrations (Fig.2). ^3H with a potential Los Alamos Canyon origin has been co-detected with Cr^{6+} in the perched and regional groundwater beneath Sandia and Mortandad Canyons [8]. Currently, no LANL outfalls release water into Los Alamos Canyon watershed, but significant natural infiltration occurs. The natural infiltration recharges along Sandia and Mortandad Canyons are substantially less than the natural infiltration recharge along Los Alamos Canyon.

Cr^{6+} concentrations in the regional aquifer exceed 50 µg/ℓ (the New Mexico groundwater standard) at several monitoring wells (Fig.1); the highest concentration is ~1000 µg/ℓ (ppb). ClO_4^- is also present in the aquifer at concentrations exceeding the established screening level of 4 µg/ℓ (Fig.1). 1,4 dioxane is present in perched-intermediate groundwater beneath Mortandad Canyon at concentrations exceeding the groundwater standard, but the contaminant is currently not detected in the regional aquifer [8].

SITE CONCEPTUAL MODEL

The site conceptual model describes the processes controlling the movement of groundwater and contaminants in the environment. The current conceptual model is explained in detail in [8], and supported by multiples lines of evidence. The establishment of the current conceptual model involved field, laboratory and modeling analyses [8]. The current understanding of the chromium distribution in the environment is presented in Tbl.1. A schematic 3D representation of the conceptual model is shown in Fig.2. At least 25% of the released chromium mass is currently in Sandia Canyon sediments (~18,000 kg); about 15,000 kg of this mass resides in the wetland at the head of the canyon (Fig.2). The chromium in the canyon sediments (including the wetland) is predominantly in reduced and non-toxic Cr^{3+} form based on X-ray Absorption Near Edge Structure (Xanes) analyses [7]. Alluvial groundwater in Sandia Canyon is recharged daily by effluent discharges and periodically by stormwater; this provides sufficient water to mobilize contaminants within the watershed. Based on surface water-balance field studies, the infiltration of alluvial water is negligible in the upper canyon sections (including the wetland); most of the infiltration occurs downgradient from SCI-1 (Fig.1) with rates potentially as high as 1-6 m/a. Currently, the groundwater infiltrating into the subsurface along the canyon bottom has Cr^{6+} concentrations substantially below the

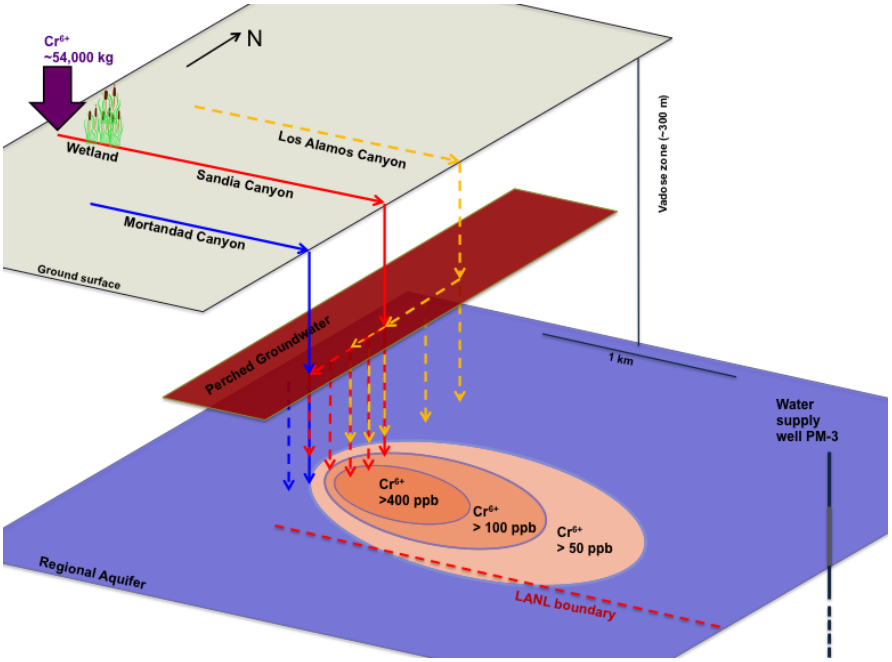

Figure 2: Three-dimensional conceptual representation of groundwater flow and contaminant transport in the subsurface beneath Los Alamos (yellow flow lines), Sandia (red) and Mortandad Canyons (blue).

groundwater standard (50 µg/ℓ). The infiltration of alluvial groundwater along Mortandad Canyon also occurs nearby, predominantly, in the area near MCOBT-4.4 (Fig.1).

Water infiltrating along the three canyons migrates through the vadose zone mostly vertically driven by gravity (Fig.2). However, perching horizons divert some of the percolating water laterally along intermediate saturated zones extending between the three canyons (Fig.2). The perching horizons are observed at the top, within, and at the bottom of lavas embedded between vadose-zone sediments (Puye Formation). The flow direction in the perched zones is predominantly to the south/southwest, perpendicular to the eastward draining canyons. Between the canyons, some of the laterally-diverted water continues to percolate vertically toward the regional aquifer; however, some of the water reaches neighboring canyons. As a result of lateral diversion along perching horizons, the greatest mass Cr^{6+} contamination reaches the aquifer to the south of Sandia Canyon, where it initially infiltrated in the subsurface (Fig.2). The reduction of water released in Sandia Canyon in the next few years will not have an immediate effect on aquifer recharge; the current rate of recharge is expected to continue for 10 years or more due to the thickness (~300 m) and flow complexity of the vadose zone. There is limited information about Cr^{6+} concentrations in the vadose zone; currently, the highest observed Cr^{6+} concentration in the vadose zone is less than 600 µg/ℓ, lower than the highest concentration observed in the regional aquifer (~1000 µg/ℓ). Considering the contaminant mixing in the aquifer, the Cr^{6+} concentrations in the lower vadose zone that cause the contamination in the aquifer must be substantially higher than 1000 µg/ℓ.

The regional aquifer is complex and heterogeneous including confined and unconfined zones [10]. The shallow portion of the aquifer (near the water table) is predominantly under phreatic (unconfined) conditions; the thickness of the phreatic zone is variable and approximately 30 to 50 m below the regional water table. The deep portion of the aquifer is predominantly under confined conditions, and it is stressed by municipal water-supply pumping (the nearby pumping wells are shown in Fig.1). The pumping appears to have little impact on the groundwater flow and transport directions along the regional water table in the study area. Model analyses indicate full to partial confinement of the deep portion of the aquifer at the chromium site is required to calibrate to hydraulic heads observed in the monitoring wells. However, the poor hydraulic communication between the deep and shallow aquifer section does not preclude the possi-

Table 1: Estimates of chromium source and mass distribution in the environment including the predicted anthropogenic chromium speciation and uncertainty bounds.

Source/Media	Cr^{6+} [kg]			Cr^{3+} [kg]			$Cr^{6+} + Cr^{3+}$ [kg]		
	mean	min	max	mean	min	max	mean	min	max
Source (original)	54,000	31,000	72,000	0	0	0	54,000	31,000	72,000
Wetland	0	0	0	15,100	4,800	22,700	15,100	4,800	22,700
Alluvial sediments (after the wetland)	0	0	0	2,900	900	4,300	2,900	900	4,300
Bandelier tuffs	2,600	300	12,800	7,900	800	38,300	10,500	1,000	51,000
Puye sediments (upper)	3,000	600	15,000	9,000	1,800	45,000	12,000	2,400	60,000
Perched zones (groundwater only)	200	100	500	0	0	0	200	100	500
Lavas (fractured basalt flows)	1,800	200	2,300	5,300	700	6,800	7,000	900	9,000
Puye sediments (lower)	1,000	300	2,000	3,000	800	6,000	4,000	1,000	8,000
Miocene sediments	200	0	1,000	500	100	3,000	700	100	4,000
Aquifer (groundwater and sediments)	1,100	300	3,300	10	1	100	1,100	300	3,400
Total in media (rounded)	9,900	1,800	36,900	43,700	9,900	126,200	53,500	11,500	162,900

bility of Cr^{6+} migration between the shallow and deep aquifer zones. Between the two zones, the hydraulic gradient has a strong downward vertical component because of water-supply pumping, creating the possibility for downward Cr^{6+} flow via "hydraulic windows," although these have not been observed.

The groundwater flow in the aquifer is generally from west to east. The hydraulic gradients are high to the west (due to elevated mountain front recharge) and to the east (close to the Rio Grande); however, the gradients are relatively low in the Cr^{6+} plume area (~0.001 m/m). The juxtaposition of zones with steep and flat hydraulic gradients complicates the analyses of the flow directions in the study area. The contour lines of the elevation of the water table (circa 2012) in the study area are shown in Fig.1. The shape of the regional water table is complex; it is affected by aquifer heterogeneity and infiltration recharge (considering the large volumes of surface water flowing along Sandia and Los Alamos Canyons). It is also likely the water table in the study area is influenced by water-supply pumping. However, current water-level records suggest limited pumping impact on the current shape of the regional water table. The low hydraulic gradient near R-28 (Fig.1) is potentially caused by the high effective permeability of the sediments in this portion of the aquifer. The water-level data suggest infiltration mounding of the water table near wells R-8, R-36, and R-42 (Fig.1). The R-8 and R-36 mounds are potentially caused by Los Alamos Canyon infiltration. The mounding near R-42 is expected to be related to infiltration recharge of the aquifer carrying the historic Cr^{6+} contamination from Sandia Canyon. The mounding may cause a portion of the Cr^{6+} plume to migrate to the north, west and south of contaminant arrival locations, enhancing the contaminant mixing in the aquifer. The size and magnitude of the water-table mounds depend on the distribution of infiltration flux and local hydrogeological properties.

Groundwater flow and contaminant transport directions in the phreatic zone are generally determined by the gradient of the regional water table (Fig.1). However, the aquifer appears to be highly heterogeneous and anisotropic due to hydrostratigraphic bedding and channelization of sedimentary deposits. Aquifer heterogeneity is expected to cause local 3D deviations in flow directions not captured by the water-level data. Aquifer heterogeneity may focus a predominant portion of the contaminant flow into aquifer areas having high permeability. In addition, advective flow paths of contaminant migration may not be strictly perpendicular to the equipotential water-table lines (i.e., parallel to the hydraulic gradients). Deviations may occur because of anisotropy of aquifer materials caused by sedimentation processes and tilting of the hydrostratigraphic units to the south-southwest with dip of ~10^{o}. These factors may cause the flow and hydraulic-gradient vectors to deviate (if the hydraulic gradient is not coincident with the principal directions of the anisotropic permeability tensor) [8]. Analyses of long- and short-term pumping tests conducted in the study area demonstrate the aquifer is heterogeneous. Pumping test data did not show pronounced aquifer anisotropy; however, the interpretation is uncertain because of the small magnitude of the pumping-test drawdowns in observation wells [8]. As shown in Fig.1, the hydraulic gradient suggests the flow direction near R-42 and R-28 is east-southeast (with possible diversions to the southeast or northeast).

However, there is uncertainty in this flow-direction estimate because of: (1) the relatively small magnitude of the hydraulic gradient in this area and (2) the 3D and heterogeneity effects that impact the pressure measurements at individual well screens (screens have different depths and lengths; none of the screens in the study area straddles the regional water table).

The footprint of contaminant arrival locations from the vadose zone to the top of the aquifer is unknown. All the existing site information including the shape of the Cr^{6+} plume (Fig.1) suggests that in the area near R-42 and R-28 either there is (1) one relatively large and continuous breakthrough area (potentially with nonuniformly distributed contaminant fluxes) or there are (2) several breakthrough areas (with different contaminant fluxes). From the breakthrough areas, the Cr^{6+} plume migration is expected to be predominantly east-southeast toward wells R-44 and R-45 (Fig.1). This general direction of Cr^{6+} transport appears to parallel the separate ClO_4^- plume originating from Mortandad Canyon infiltration. The ClO_4^- plume is defined by observations in wells R-15, R-61, and R-50 (Fig.1). However, the shapes of the contaminant plumes and the groundwater flow directions based on hydraulic gradients in Fig.1 are not entirely consistent; this suggests that aquifer anisotropy and heterogeneity and/or infiltration mounding effects not captured in the existing water-level data may have important impacts on contaminant migration and plume shapes.

Cr^{6+} migration in the vadose zone and the regional aquifer is impacted predominantly by advection, dispersion, diffusion, retardation and redox reactions (specifically reduction). The contaminant mass moves predominantly by advection with the groundwater flow. Mechanical dispersion within the vadose zone and aquifer is enhanced by the pronounced heterogeneity of the subsurface materials. The diffusion of Cr^{6+} between zones with higher and lower permeability is expected to retard the effective transport velocity; after the Cr^{6+} concentrations in the more permeable zones decrease due to diminishing contaminant source (the release was between 1956 and 1972), back diffusion of Cr^{6+} from low into high permeability zones is expected to retard the long-term decline of Cr^{6+} concentrations in the vadose zone and the regional aquifer [8]. The geochemical interactions of chromium with subsurface materials are expected to have important effects on contaminant transport by causing Cr^{6+} reduction and retardation. The chromium retardation from adsorption or chemical reactions between Cr^{6+} in the solid and water phases does not reduce the contaminant mass but slows down Cr^{6+} contaminant transport. However, chromium reduction from chemical reactions converting Cr^{6+} into less toxic and less mobile Cr^{3+} effectively decreases the contaminant mass in groundwater. The reduced Cr^{3+} precipitates out and becomes functionally immobile; as a result, it is no longer considered a portion of the contaminant plume. Reverse oxidization reactions of Cr^{3+} to Cr^{6+} at the site are not well understood; currently, they are considered to be negligible because of potentially slow kinetics of the involved geochemical reactions and lack of oxidant minerals such as MnO_2 in the aquifer sediments. The Cr^{6+} reduction in the environment is demonstrated using Cr stable isotope analyses [7,8]. The isotope data indicate reduction has occurred between the surface and the regional aquifer, but they do not show significant Cr^{6+} reduction in the aquifer; however, analytical uncertainties may account for the anthropogenic Cr^{3+} mass due to reduction in the range between 1% and 10% of the current Cr^{6+} mass in the aquifer. Although the reducing capacity of the lavas in the vadose zone is significant, either the kinetics of reduction are relatively slow or the reduction capacity has been overwhelmed along the predominant flow paths by the large mass and high historic concentrations of Cr^{6+} that passed through the basalt. The analyses of stable isotope data for evaluation of the Cr^{6+} reduction are further complicated due to existence of natural and anthropogenic chromium in the subsurface; the natural (non-anthropogenic) Cr^{6+} concentrations in the regional aquifer are between 5-8 μg/ℓ. Further analyses are being conducted to better constrain uncertainties associated with Cr^{6+} reduction at the site.

Estimates of chromium source and mass distribution in the environment including the predicted Cr speciation and uncertainty bounds are presented in Tbl.1. The estimates for the contaminant mass in the vadose zone are based on analyses of pore water and rock samples from boreholes [7]. The estimates for the Cr^{6+} mass in the aquifer are based on numerical model simulations (discussed further below).

The site data suggest groundwater infiltrates from the ground surface to the top of the regional aquifer (vertical distance ~300 m) with infiltration rates on the order of 1 to 6 m/a, and travel times between 5-60 years; the effective groundwater flow velocity through the vadose zone is ~5-60 m/a. The uncertainty bound of groundwater travel time through the vadose zone accounts for potential complex flow paths with low and high groundwater flow velocities. The mean travel time for a dominant portion of the groundwater infiltrating trough the vadose zone is expected to be ~20-40 years. Cr^{6+} transport through the vadose zone is expected to be retarded because the Cr^{6+} is slowed by diffusion between high and low permeability zones, and geochemical reactions with subsurface materials. Based on hydraulic gradients and properties of the aquifer, groundwater flow in the aquifer is expected to occur with pore-water (linear) velocity of about 40-50 m/a (discussed further below); the distance between R-28 and R-44/R-45 is ~400 m; therefore the travel time will be on the order of 10 years. These velocity estimates are generally consistent with the timing of the Cr^{6+} releases (1956-1972) and the Cr^{6+} detection in the aquifer (since 2004). The currently observed contamination in the aquifer (Fig.1) potentially represents a steady-shape plume caused by equilibrium between the contaminant flux arriving from the vadose zone and the groundwater flow in the aquifer. The concentrations at most of the wells have been relatively steady; e.g. R-28 concentration has been around 400 µg/ℓ since 2004. However, there are also concentration transients with differing magnitudes and trends that may be caused by local variations in the geochemical conditions (including borehole drilling effects) and plume non-uniformity. The concentration transients continue to be closely monitored, analyzed, and compared to model predictions to assess plume stability and detect any unexpected fluctuations.

METHODOLOGY

A methodology has been developed to identify contaminant-arrival (breakthrough) zones at the top of the regional aquifer and to optimize the monitoring-well network. The methodology is general and can be applied at other sites. It is based on coupling of a state-of-the-art analytical solver simulating 3D groundwater transport with advanced optimization (calibration), sensitivity analyses, and uncertainty quantification techniques for analysis of the model results. This allows for efficient and robust exploration of uncertainties and estimation of uncertainties in model predictions. The methodology can consider wide ranges of uncertainties related to conceptual models, model parameters, contaminant-arrival (breakthrough) zones, and transients in the contaminant mass flux arriving at the top of the regional aquifer. The methodology can account for uncertain direction and magnitude of groundwater velocity, including vertical downward flow. It can represent single and multiple breakthrough zones simultaneously affecting aquifer concentrations. The contaminant fluxes at each zone can be steady or transient with different characteristics. However, the methodology cannot account for heterogeneity or transients in groundwater flow. To account for aquifer heterogeneity and transients, a numerical model is used in addition to the analytical model. This approach has been successfully applied in [8]; however, the numerical modeling is orders of magnitude more computationally demanding.

The goals are to (1) calibrate the model against available Cr^{6+} concentration data observed in the regional aquifer, (2) estimate potential zones of contaminant arrival at the regional water table based on the site data, (3) estimate spatial and temporal (past and current) distributions of Cr mass in the aquifer and their associated uncertainties, and (4) evaluate detection efficiency of the existing monitoring network. These are achieved through a formal model calibration process that accounts for model, parametric, and observation uncertainties. In this process, all the models with parameters within predefined uncertainty bounds and capable of reproducing all the observed concentrations within predefined uncertainty bounds are considered acceptable. The acceptable models are analyzed to explore uncertainties in model parameters and model predictions, and to evaluate detection efficiency of the monitoring well network.

A single computational tool is designed to perform all the analyses efficiently utilizing available computational resources though serial or parallel execution. The tool is embedded in the code MADS (Model Analyses for Decision Support; http://mads.lanl.gov) [11]. MADS is C/C++ code designed to be an

open-source framework for model-based decision support employing system and physics simulation models. MADS performs various types of model analyses, including sensitivity analysis, parameter estimation, uncertainty quantification, model calibration, selection, and averaging. Various demos, execution examples, and a tutorial are available at the MADS website.

Contaminant transport model

The analytical solution for concentration $c(x,y,z,t)$ of a contaminant released at a finite dimension source with a box shape in an aquifer with coordinates $(0,0,z_0)$ has the following form [12,13,14]:

$$c(x,y,z,t) = c_0 + \frac{1}{8\pi\theta_T x_S y_S z_S}\int_0^t I(t-\tau)\exp(-\lambda\tau)\left[erfc\left(\frac{x-\frac{1}{2}x_S-v\tau}{2\sqrt{\alpha_L v\tau}}\right)-erfc\left(\frac{x+\frac{1}{2}x_S-v\tau}{2\sqrt{\alpha_L v\tau}}\right)\right]\left[erfc\left(\frac{y-\frac{1}{2}y_S-v\tau}{2\sqrt{\alpha_{TH} v\tau}}\right)-erfcy+12yS-v\tau 2aTHv\tau erfcz-z0+zS2aTVv\tau-erfcz-z02aTVv\tau+erfcz+z0+zS2aTVv\tau-erfcz+z02aTVv\tau d\tau\right] \quad (1)$$

where c_0 is background concentration, α_L, α_{TH}, and α_{TV} are the longitudinal, transverse horizontal, and transverse vertical dispersivities [L], respectively; λ is the half-life decay constant [T^{-1}]; θ_T is water-filled porosity [−], and $I(t)$ is the contaminant mass flux (mass per unit time) [MT^{-1}]. The contaminant flux $I(t)$ can be transient and vary in any functional or piecewise fashion. The effective contaminant velocity v is steady, uniform, and along the x solution axis. The half-life decay constant λ is applied to represent zero-order chemical reactions reducing Cr^{6+} into Cr^{3+} with a constant reaction rate. Eq.1 represents flow in a uniform aquifer bounded at the top ($z = 0$) and with infinite vertical thickness and lateral extent. If $z_0 = 0$, the source location will be at the top of the aquifer (at the regional water table). The region where contaminant-arrival flux is released is a parallelepiped (box) with sizes x_S, y_S, and z_S along each axis. The equation above suggests that if contaminant mass flux is steady, after some time the contaminant concentrations will reach steady values as well. To account for multiple contaminant sources, the respective solutions obtained using Eq.1 are superimposed multiple times. In these cases, each source is characterized with different dimensions x_S, y_S, and z_S and different contaminant fluxes $I(t)$.

The aquifer anisotropy in the horizontal plane is captured by taking into account the uncertainty in the direction of advective transport. This is represented by a flow direction angle φ, which is applied to rotate the x and y axes of the analytical solution relative to the source location. The angle is adjusted in the calibration process to match concentration data. The aquifer anisotropy in the vertical direction is characterized through selection of dispersivity coefficients. The ratio between horizontal and vertical transverse dispersivities is representative of vertical anisotropy; the layering of aquifer material is expected to cause lower vertical transverse dispersivity. By varying the ratio of the dispersivities, the impact of aquifer anisotropy on the contaminant transport is effectively captured.

The analytical solution of contaminant transport based on Eq.1 for single and multiple contaminant sources is obtained using the code MADS [11]. Various U.S. Geological Survey (USGS) codes for simulation of contaminant transport (such as ART3D, BIOSCREEN) can be applied as well, but MADS provides a larger range of computational options and capabilities. In the past, the USGS codes used the solution proposed by [15]; however, this solution has been shown to be inaccurate [16,17]. Recently, the analytical solutions applied in the USGS codes have been corrected.

Single and multiple (up to 3) contaminant-arrival (breakthrough) zones are considered. The Cr^{6+} flux is assumed to be uniform in time; this assumption is generally consistent with the current observations of chromium concentrations at most of the aquifer monitoring wells, which are also relatively steady since 2004. Steady-state concentrations are not expected to continue indefinitely because the original chromium source released to Sandia Canyon had a finite release period (from 1956 to 1972); however, the slow diffusion and/or desorption of Cr^{6+} from subsurface materials may cause a slow decline of the contaminant fluxes in the future. Therefore, the assumption of a steady contaminant flux can be applied as an approx-

Table 2: Model parameters for analytical simulation of contaminant transport in the regional aquifer.

Model Parameter	Unit	Initial Estimate	Calibration Range	
			Minimum	Maximum
Background concentration c_0	$\mu g/\ell$	5	Fixed	
Source coordinate x	m	—	498,450	499,700
Source coordinate y	m	—	538,850	539,550
Source coordinate z (at top of the aquifer)	m	0	Fixed	
Source dimension x_S	m	200	1	1500
Source dimension y_S	m	200	1	1500
Source dimension z_S (1 m below the top of the aquifer)	m	1	Fixed	
Contaminant flux to the regional aquifer I	kg/a	10	0.01	100
Contaminant-arrival time t_0	a	1980	1960	2012
Contaminant cessation time t_1	a	2160	Fixed	
Half-life decay λ (accounting for potential Cr^{6+} reduction to Cr^{3+})	a^{-1}	10^{+6}	10^{-1}	10^{+6}
Flow angle φ	$degrees$	−24	−90	0
Effective water-filled porosity θ_T	-	0.3	Fixed	
Effective pore (linear) velocity of contaminant migration v (accounting for potential Cr^{6+} retardation)	m/a	40	1	600
Longitudinal dispersivity α_L	m	10	10	200
Horizontal transverse dispersivity α_{TH}	m	5	1	100
Vertical transverse dispersivity α_{TV}	m	0.1	0.01	5

imation to evaluate the current distribution of Cr^{6+} mass in the aquifer. In the case of multiple contaminant-arrival zones, each zone can have a different initial arrival time and different steady-state flux. In this way, multiple contaminant-arrival zones can effectively represent transients in the Cr^{6+} mass flux and arrival time to the aquifer. Because ambient groundwater flow velocities in the aquifer are relatively high, the recent Cr^{6+} concentrations at the contaminant-arrival zone, rather than past transients, predominantly cause the currently observed concentrations at the monitoring wells. As a result, it is difficult to evaluate what past Cr^{6+} concentrations were upon arrival at the regional aquifer. Nevertheless, the analytical model of chromium transport in the aquifer is applied to evaluate the maximum contaminant mass that may have arrived at the aquifer between 1960 and 2012 and still yield concentrations consistent with the current observations.

The best approach to account for all the complexities at this site is through development of 3D numerical models. Such models are developed for this site in [7] and [8]. The models account for 3D groundwater flow effects (including aquifer recharge and municipal water-supply pumping), aquifer heterogeneity, and coupled vadose zone and aquifer flow and transport. However, the flexibility to efficiently explore large uncertainties in conceptual elements and model parameter space with the analytical model is important. The major limitations in applying the analytical solution rather than a numerical model for simulation of 3D contaminant transport are that the analytical solution is constrained: (1) the aquifer has uniform hydrogeological properties, (2) groundwater flow is steady state and uniform, and (3) pumping effects from water-supply wells cannot be accounted for. The major benefits in applying the analytical solution rather than a numerical model are (1) execution time is very fast (less than a second); (2) the analytical solution accurately represents aquifer dispersion (numerical models generally overestimate dispersion) [6,7]; (3) the aquifer anisotropy can be efficiently captured; and (4) transients in the input contaminant flux and the observed concentrations at the monitoring wells can be easily incorporated in the model. It is important to note the execution time is critical for the performance of the analyses presented below. The estimation of the potential zones of contaminant arrivals requires on the order of 10^7 to 10^8 analytical model executions requiring more than 1 year of wall-clock execution time. A single execution of a numerical model with similar scale and complexity requires ~10 minutes; therefore, similar analyses may have required on the order of 600 years of wall-clock execution time.

Model parameters

The parameters applied in model simulations are listed in Tbl.2; the parameter initial estimates and calibration ranges are estimated based on the available site-specific data and literature data. The *x* and *y* coordinates of the potential contaminant-arrival locations vary in a rectangular area that encompasses a region around R-42 and R-28 (Fig.3b). The contaminant-arrival zone(s) has unknown lateral location and lateral size but has a fixed vertical location (z = 0 m) and size (z_S = 1 m). The assumed 1-m-thick contaminant-arrival region represents the zone of initial mixing of vadose-zone contaminants with aquifer groundwater. Seasonal fluctuations of the regional water table may also influence the vertical dimension of this region. The lateral location (coordinates) and lateral dimensions of the contaminant-arrival region are adjusted during model calibration to match the calibration data.

Contaminant mass flux from the vadose zone is assumed steady and equal to a fixed value [kg/a] within a specified time window from a starting time t_0 [a] to an ending time t_1 [a]. The plausible mass flux values are defined to be within a wide range to account for existing uncertainty (Tbl.2). The time of arrival of contaminants at the top of the aquifer, t_0, is varied between 1960 and 2012 to accommodate the uncertainty associated with vadose-zone transport velocities (chromium was released in Sandia Canyon from 1956 to 1972). The time at which contaminants cease to arrive in the regional aquifer, t_1, is fixed (2160) and does not influence the simulations performed below. Contaminant half-life decay representing chromium reduction is not included in most of the simulations by setting the half-life decay coefficient to a large value ($\tau = 10^{+6}$ a^{-1}). However, for some of the simulations discussed below, the half-life decay coefficient is adjusted by the model during the calibration process to account for Cr^{6+} reduction.

Setting initial estimates and uncertainty ranges of the pore velocity is based on a detailed analysis of the available data [8]. The aquifer permeability in monitoring wells near the chromium plume ranges between 0.3 and 41 m/d, with a best estimate of about 12 m/d. No site-specific estimates of the effective transport porosity are available; based on literature data [17], porosity of sandstones and gravels is expected to vary between 0.1 and 0.2 with a best estimate of 0.15. The best estimate of the effective water-filled porosity of the aquifer pore space is 0.3; this parameter characterizes the available water volume for contaminant mixing. In contrast, the effective transport porosity characterizes the connected pore space controlling the advective contaminant flow through the aquifer. The hydraulic gradient in the vicinity of the chromium plume is on the order of 0.001, with an uncertainty range from 0.0005 to 0.002. Based on all these data, the best estimate for the advective transport velocity (also called pore or linear velocity) within the aquifer of a nonreactive contaminant is on the order of 40-50 m/a with an uncertainty range between 1 and 600 m/a (Tbl.2). Cr^{6+} is not expected to be a nonreactive contaminant. Cr^{6+} retardation and reduction are geochemical processes that may impact the contaminant concentrations and migration velocity. Therefore, the uncertainty range (1 to 600 m/a) in the effective Cr^{6+} migration velocity also accounts for uncertainties in the geochemical reactions influencing contaminant mobility.

The contaminant-flow direction is represented by the angle φ between the *x* axis and the flow vector. The angle can vary from 0 (flow due east) to −90 (due south), allowing for a wide range of uncertainty in the advective flow direction. No site-specific estimates of the dispersivity coefficients are available; initial estimates and uncertainty ranges are based on literature data that take into account the scale at which contaminant transport occurs [18,19,20]. The longitudinal dispersivity is typically $1/10^{th}$ of the distance traveled by the contaminant; typically, the transverse horizontal and vertical dispersivities are assumed to be $1/10^{th}$ and $1/100^{th}$ of the longitudinal dispersivity, respectively. All these parameters are assumed to be uncertain; the model adjusts these parameters to calibrate against observed chromium concentrations. There are alternative ways to conceptualize interdependencies between dispersivities and their relationship with the travelled distance. In a previous analysis [7], the dispersivities were assumed to be independent. In that case, the longitudinal, transverse lateral, and traverse vertical dispersivities were allowed to vary independently of each other. As a result, the model analyses presented in [7] allowed for simulations where transverse dispersivities are larger than the longitudinal dispersivity. This was acceptable because aquifer

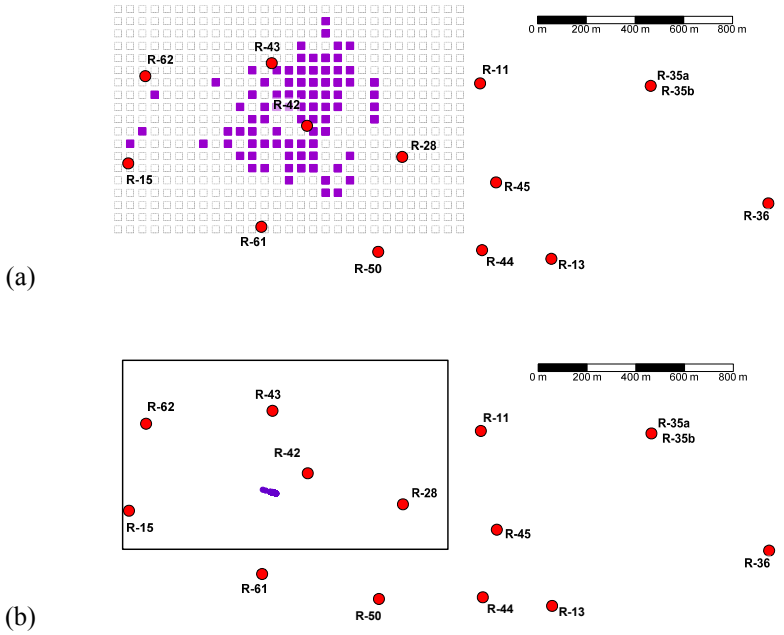

Figure 3: Estimated contaminant-arrival locations (purple dots): (a) 2009 analysis without R-50, R-61, and R-62 data (grey squares represent all the analyzed contaminant-arrival locations); (b) 2012 analysis with R-50, R-61, and R-62 data (black rectangle represents the uncertainty bounds in contaminant-arrival locations). Purple dots represent the coordinates (centroids) of the arrival breakthrough zones; dot sizes do not represent the size of breakthrough zones.

heterogeneity and multiple arrival locations can produce plumes that are more dispersed transversely than longitudinally. Here, the analyses are performed assuming coupled dispersivities; this does not allow transverse dispersivities to become larger than the longitudinal dispersivity. This is because the new analyses allow for multiple contaminant-arrival zones that can represent more realistically the apparent plume dispersion in the aquifer. All these conceptual representations of related aquifer dispersivities are available as alternative computational options in MADS [11].

The model analyses are performed allowing for multiple contaminant-arrival zones. Each zone is defined with a separate set of coordinates, sizes, and contaminant fluxes; the same aquifer properties are applied to simulate contaminant migration from each contaminant-arrival zone (flow velocity, etc.).

Model calibration

The Cr^{6+} concentrations in the aquifer observed at the monitoring wells near Sandia Canyon are applied as calibration targets. However, the Cr^{6+} concentrations used to calibrate the model are uncertain. Uncertainties in the calibration data are caused by various factors [7]. The important sources of uncertainty are (1) background values of Cr^{6+} concentrations in the aquifer, (2) differences in local geochemical conditions near the monitoring wells, and (3) fluctuations and trends in the observed Cr^{6+} concentrations at the monitoring wells near Sandia Canyon. For each calibration target, an acceptable range is defined. The goal is to obtain model prediction with Cr^{6+} concentrations within the acceptable range. A formal process for estimating calibration targets and their respective acceptable (uncertainty) ranges is developed in [7]. The calibration data set is extensive: it includes 124 time-dependent concentration observations in 23 monitoring screens located in 17 wells. The data captures annually-averaged concentrations from 2004 until 2012. The number of calibration targets per well varies between 1 and 9. Fig.1 presents the mean values of the 2012 calibration targets. All the calibration targets and the respective acceptable ranges are listed in [8; Table J-4.0-1].

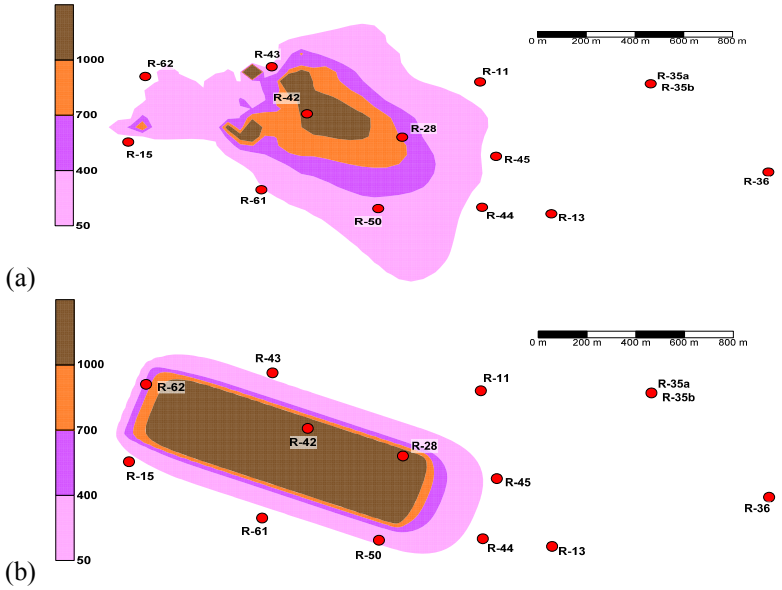

Figure 4: Estimated mean Cr^{6+} concentration [μg/ℓ] at the water table based on averaging all the acceptable model solutions: (a) 2009 analysis without R-50, R-61, and R-62 data; (b) 2012 single-source analysis with R-50, R-61, and R-62 data.

The model calibrations are executed multiple times for a series of different initial guesses for the contaminant-arrival location(s). The initial guesses are random values within the lateral bounds presented in Fig.3b. The calibration algorithm is allowed to adjust the location of the contaminant-arrival locations jointly with other model parameters. If the contaminant-arrival locations and model parameters (Tbl.2) are successfully adjusted, and the model predictions are within the acceptable calibration ranges, an acceptable model with a respective set of acceptable model parameters is identified. Once the optimization process reaches an acceptable solution the optimization is terminated. This approach allows for efficient and robust exploration of the parameter uncertainties. It is important to emphasize most of the model parameters were adjusted during model calibration (Tbl.2). The optimization approach can be characterized as a multi-try or multi-start technique because the optimization is initiated from multiple random initial guesses for the model parameters.

The objective function applied during optimization is computed as a sum of the squared differences between observed and simulated concentrations at all the well screens. The calibration is performed using local and global (Levenberg-Marquardt [21,22,23] and Squads [23]) optimization techniques, and analyses of model uncertainties are performed using an agent-based global uncertainty and sensitivity (ABAGUS) technique [25]; all these methods are embedded in the code MADS [11].

RESULTS

For the case of a single contaminant-arrival (breakthrough) zone, the identified acceptable contaminant-arrival locations at the top of regional aquifer are estimated by studies performed in 2008 [6], 2009 [7] and 2012 [8]; these reports represent continued advancements in the tools and approaches applied to provide site-specific decision support. The analyses presented in [6] and [7] employed an approach where the breakthrough coordinates were fixed along predefined lateral grids (100×100 m^2 and 50×50 m^2, respectively). This provided limitations on the implemented analyses but also helped the optimization process by reducing the number of degrees of freedom by two; all the model parameters were optimized except for the source coordinates. The results obtained in [7] are shown in Fig.3a; out of 551 potential breakthrough locations, the analysis identified 83 as acceptable (solid purple dots). The spatial discontinuity of the ac-

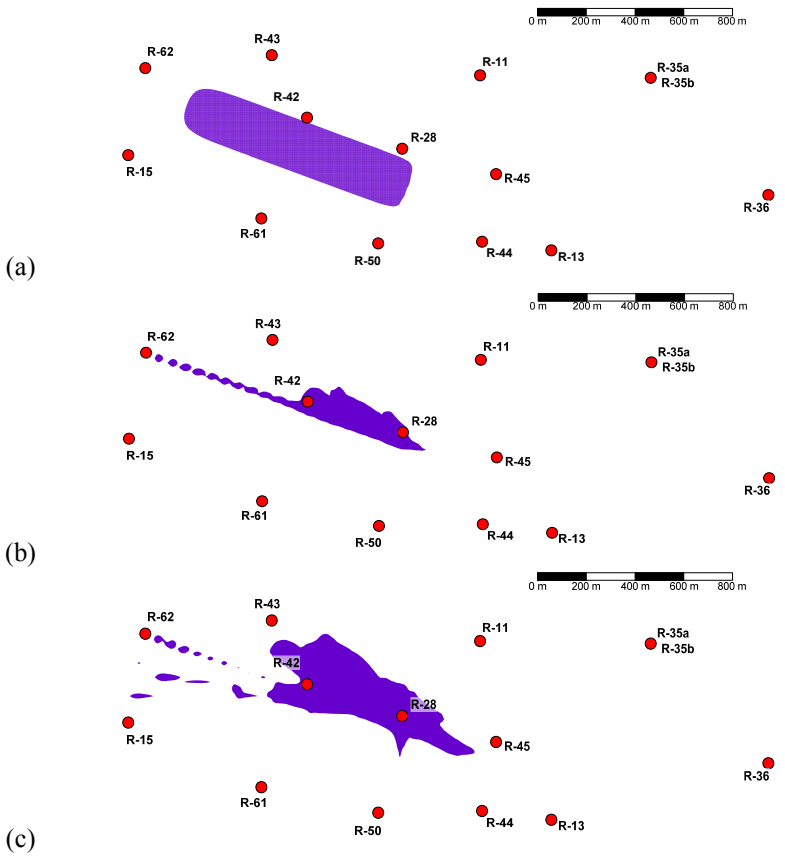

Figure 5: Regions along the top the regional aquifer where the calculated Cr^{6+} concentrations exceed 1500 µg/ℓ based on averaging of all the acceptable model solutions: (a) one (b), two and (c) three breakthrough zones

ceptable locations demonstrates complexity of the explored parameter space. The 2009 analyses did not include the data collected at recently-installed monitoring wells R-50, R-61, and R-62. In fact, the analyses were applied to place these wells in a way in which the newly collected data would reduce predictive uncertainty [26]. Fig.4a shows the best estimate of the Cr^{6+} concentrations along the regional water table (circa 2009). The best estimate is computed by averaging the concentrations of all the acceptable model-predicted Cr^{6+} plumes. Fig.4a predicts that the contaminant plume may have extended to the west (in the area of R-62) and to the southeast (in the area of R-61 and R-50) from the R-42/R-28 area. These model predictions were confirmed by the data collected at these wells when they were drilled (Fig.1).

The work conducted in 2012 [8] implemented high-performance computing and novel robust model analyses techniques for optimization and uncertainty quantification, which allow for solving problems with larger degrees of freedom. The new work also included a larger number of calibration targets, new Cr^{6+} calibration targets obtained from R-50, R-61, and R-62, and more detailed characterization of the temporal Cr^{6+} concentration data at all the monitoring wells due to longer data records. The new work also included a larger set of unknown model parameters, multiple contaminant-arrival zones, and parameters characterizing the potential Cr^{6+} reduction and reaction in the aquifer. The new work did not utilize parameter constraints. The initial guesses for the x and y coordinates of the breakthrough location are randomly selected within a rectangular area shown in Fig.3b. For the case of a single breakthrough zone, Fig.3b presents the breakthrough coordinates of all 492 acceptable models; the locations almost overlap because all the acceptable models are practically equivalent. In Fig. 3a and 3b, dots represent the coordinates (centroids) of the arrival breakthrough zones; the dot sizes do not represent the size of the breakthrough zones. A com-

parison of Figs. 3a and 3b demonstrates the new data collected at R-50, R-61, and R-62 effectively constrain the uncertainty in the contaminant arrival locations. This proves consistency in the modeling analyses and a trend of reduction of uncertainty in the model predictions with the drilling of new wells and collection of new data. Fig.4b shows the best estimate of the acceptable Cr^{6+} concentrations along the regional water table (circa 2012). The best estimate is computed by averaging the concentrations of all the acceptable model-predicted Cr^{6+} plumes; note that in this case, all these plumes are almost equivalent. The contaminant-arrival zone represents a laterally-elongated rectangle located south of R-42. The large size of the single-source zone suggests that multiple contaminant-arrival zones may also yield acceptable solutions that will calibrate to the observed concentrations.

Figure 5 shows model predicted regions along the regional water table where Cr^{6+} concentrations are calculated to exceed 1,500 μg/ℓ (circa 2012). The results are obtained by averaging the concentrations of all the acceptable model-predicted Cr^{6+} plumes for the case of one, two and three contaminant-arrival zones. More than 5000 acceptable models are generated, and many of the obtained plumes are similar. The solutions presented in Fig.4b and Fig.5a are equivalent. The single breakthrough-zone case (Fig.5a) represents the worst-case scenario in terms of spatial extent of high Cr^{6+} concentrations (>1,500 μg/ℓ). Note that this representation of the plume illustrates the concentration along the top of the aquifer; it differs from the plume shown in Fig. 1, which is based on data from well screens located at different depths below the water table. The solutions for two and three contaminant-arrival zones are consistent; dominant breakthrough zones causing high Cr^{6+} concentrations are expected to be near R-42 and R-28 with potential breakthrough locations upgradient from R-42/R-28 in the area near R-62.

Table 3 lists the mean estimates associated with the successfully calibrated models. The values are compared with the 2009 results based on similar analyses but utilizing a limited set of calibration data [8]. The newly obtained results and the previous results are reasonably consistent. Most importantly, the new analysis predicts a larger present-day mass of chromium in the aquifer: 1100 kg total has been introduced in the aquifer since the contaminant was released; this also represents the total mass currently distributed within the aquifer. The uncertainty range of this estimate is between 200 and 3,000 kg; for the case of a single contaminant-arrival zone, the mass is well constrained between 960 and 1,020 kg.

DISCUSSION

The model analyses demonstrate that the spatial extent of the Cr^{6+} plume in the regional aquifer is well constrained. The existing site data provide sufficient constraints to estimate the contaminant arrival zones at the top of the aquifer. The analyses suggest the existing monitoring network provides sufficient information about the plume behavior, and no new monitoring wells are currently needed.

Based on the interpretation of the regional water-level data and the model analyses presented here, the best estimate of the groundwater flow direction is about 20 degrees south of east (−20°); this observation is consistent with the current conceptualization of both Cr^{6+} and ClO_4^- plumes. This direction is potentially aligned with the hydraulic gradient. Alternatively, some of the models converged with groundwater flow direction of about 65 degrees south of east (−65°) downgradient from R-28, producing more pronounced diversion to the south (towards R-50); however, this scenario requires pronounced aquifer heterogeneity and/or anisotropy. More southerly groundwater flow directions may also be caused by municipal water-supply pumping and/or infiltration recharge (Fig.1).

As discussed above, the groundwater transport velocity in the aquifer near R-28 may be on the order of 40 to 50 m/a or even higher. If the contaminant-arrival location is near R-42, it may take less than 8 years for contaminants to reach R-28 (the distance between the two wells is ~400 m). Because relatively short travel times to R-28 are expected, it is not surprising that Cr^{6+} concentrations at R-28 have been relatively stable since 2004 when chromium was initially detected at R-28. This finding also suggests the contaminant plume has reached a steady condition in the region between the potential contaminant-arrival location and well R-28. In addition, because of the relatively short distance between R-28 and potential downgradient

Table 3: Average model parameters estimated as a result of the model calibration versus chromium concentration data observed at the regional monitoring wells near Sandia Canyon

Model Parameter	Unit	Average parameter estimates	
		2009 [7]	2012 [8]
Source coordinate x	m	499150	499040
Source coordinate y	m	539000	539182
Source dimension x_S	m	27	430
Source dimension y_S	m	468	380
Contaminant flux to the regional aquifer I	kg/a	18	22
Contaminant-arrival time t_0	a	1977	1969
Flow angle φ	$degrees$	-7	-34
Effective pore (linear) velocity of contaminant migration v	m/a	23	14
Longitudinal dispersivity α_L	m	1	24
Horizontal transverse dispersivity α_{TH}	m	6	1
Vertical transverse dispersivity α_{TV}	m	1	0.1
Total contaminant mass	kg	550	1100

wells (500 m to R-44 and 400 m to R-45; Fig.1), it may also be expected that the contaminant plume has reached or is approaching a steady-state shape condition at R-44 and R-45. The model analyses of the observed relatively low concentrations at R-45, R-44, and R-13 have several possible explanations:

- small mass fluxes at contaminant-arrival zones located relatively close to all of the wells with the high concentrations at R-62, R-50, R-42 and R-28; this is not a very plausible scenario because it implies the wells are coincidently drilled downgradient from the potential contaminant-arrival zones;
- contaminant flow diversion to the northeast or to the southeast of R-45, R-44, and R-13 due to aquifer heterogeneity or infiltration recharge mounding;
- relatively slow contaminant flow (due to slower than currently expected groundwater flow or contaminant retardation); in this case, the major portion of the plume has not yet arrived at R-45, R-44, and R-13; the effective pore velocity should be substantially retarded, potentially as low as 4 m/a;
- contaminant plume dispersion resulting from aquifer heterogeneity; and
- chromium retardation and/or reduction in the regional aquifer.

The model analyses performed here demonstrate that if the current contaminant-arrival mass flux at the top of the regional aquifer remains steady, the R-42/R-28 concentrations are expected to remain steady as well. If there is substantial chromium reduction in the aquifer materials, a larger contaminant mass than shown in Tbl.3 may have reached the aquifer. However, the reduced mass (Cr^{3+}) would become immobile and not be evident in the measured groundwater concentrations. Therefore, it is important to constrain uncertainty bounds on the potential chromium reduction capacity of the aquifer materials to better predict future chromium transport.

The model analyses identified more than 5000 alternative models that are consistent with the available data. Many of these models are implausible. The set of multiple acceptable models consistent with the available data can be grouped into the following three categories (scenarios) related to the general behavior of the simulated contaminant plumes:

1. A subset of model scenarios is characterized by (1) single or multiple contaminant-arrival zones near the wells with the highest concentrations (R-42, R-28, R-62, and R-50) and (2) no chromium retardation/reduction in the regional aquifer. In these cases, the model accurately reproduces the observed concentrations; the model predicted aquifer concentrations relatively quickly reach steady values. Under this model scenario, most of the currently observed concentrations will remain steady in the future and will not exceed 50 μg/ℓ; the concentration at R-13 may increase to ~25 μg/ℓ. However, these models require that a relatively small amount of chromium mass has reached the aquifer (~300 kg total or less).

2. A subset of alternative models is characterized by (1) single or multiple contaminant-arrival zones (1–3) upgradient from the wells with the highest concentrations (R-42, R-28, R-62, and R-50) and (2) chromium reduction in the aquifer ($\lambda = 10\ a^{-1}$ or smaller). In these cases, the model accurately reproduces

the detected concentrations. According to the model, the concentrations will remain steady in the future; however, a larger chromium mass may have reached the aquifer (~4,000 kg or more), but much of that mass will be stable and immobile as Cr^{3+}.

3. Another subset of cases is characterized by (1) single or multiple contaminant-arrival zones (1–3) upgradient from the wells with the highest concentrations (R-42, R-28, R-62, and R-50) and (2) no chromium reduction in the aquifer. In these cases, the model accurately reproduces the observed concentrations. However, the concentrations are predicted to increase above 50 μg/ℓ in the downgradient wells such as R-44, R-45, and R-13 in the near future.

These three scenarios are potentially equally probable based on the simulation results. It is important to note the observed concentration at R-62 (200 μg/ℓ; Fig.1) may suggest there is a contaminant-arrival zone near R-62 in addition to the contaminant-arrival zone(s) associated with the contaminants observed at R-42/R-28. However, all the calibration data also can be matched with a model that has a single, elongated contaminant-arrival zone. The best model prediction for the case of a single contaminant-arrival zone is presented in Fig.3b, and it accurately matches the R-62 data. However, the model predictions obtained using multiple contaminant-arrival zones produce better representations of the observed Cr^{6+} concentrations at the monitoring wells when compared to the single contaminant-arrival case. Therefore, a conceptual model of multiple contaminant-arrival zones can be considered more feasible. However this conclusion is based on a model assuming uniform groundwater flow. Therefore it is still feasible to have a single large contaminant-arrival zone coupled with more nonuniform contaminant flow in the aquifer due to heterogeneity.

According to the model analyses, it is not feasible for contaminant-arrival zones beneath the Sandia Canyon wetland (Fig.2) to cause currently observed concentrations in the area near R-62, R-42, and R-28 (the wetland is located about ~4.5 km upgradient from R-62). If a contaminant plume originates in the aquifer beneath the wetland and the aquifer is relatively uniform (no pronounced channeling of the contaminant flow), it cannot be expected that more than 10 μg/ℓ of the currently detected chromium in R-62 originates from beneath the wetland. Higher contaminant mass may have contributed to the currently observed concentrations at R-62, R-42, and R-28, if the potential contaminant-arrival zone at the aquifer is located closer to R-62. It should be noted that having additional vadose-zone flow paths and contaminant-arrival zones (some of the vadose-zone flowpaths may have not reached the regional aquifer) upgradient of R-62 increases the potential for chromium reduction in the subsurface because the chromium mass can interact with a larger rock volume. This may be an important effect on the current contaminant mass-balance analyses (Tbl.1).

The pore (linear) groundwater flow velocity in the regional aquifer beneath the Sandia Canyon wetland is potentially higher than the velocity in the area of R-42 and R-28 because of the much higher hydraulic gradients in the aquifer. The best velocity estimate is on the order of 100 m/a with an uncertainty range of 36 to 365 m/a. Assuming a velocity of 100 m/a in the model analyses, a single contaminant-arrival zone to the aquifer near the wetland may carry a mass flux to the aquifer at a rate of ~20 kg/a and produce concentrations close to background at all the downgradient wells. If the groundwater flow velocity in the aquifer is 36 to 365 m/a, the potential contaminant flux is ~8 to 80 kg/a, respectively. In all three cases, the concentration in the aquifer near the contaminant-arrival zone is predicted to be less than 50 μg/ℓ (~20 μg/ℓ). The goal here is to explore plumes that are highly dispersed and will produce close to background concentrations in the aquifer. The analysis provides an answer to the question "What is the highest mass flux to the regional aquifer near the wetland that can remain undetected by the current monitoring well network?"

The model analyses are applied to address the question "Is it possible to have a 'stagnant' plume characterized by relatively low contaminant transport velocity?" However, this scenario practically requires multiple contaminant-arrival zones collocated with most of the monitoring wells detecting elevated chromium concentrations. This scenario also requires substantial reduction of the Cr transport velocity relative to the groundwater pore velocity as a result of hydrogeological and geochemical processes (the site data suggests the pore groundwater velocity is relatively large in the central portions of the Cr plume).

CONCLUSIONS

Plume characterization is a challenging and nonunique problem because multiple models and contamination scenarios can be consistent with the available site data and knowledge. Exploration of the conceptual, parameter, and observation uncertainties is challenging and requires substantial computational time and robust computational algorithms. Model analyses presented here explored solutions with up to three contaminant-arrival zones at the top of the regional aquifer. Each contaminant-arrival zone is characterized with unknown location, size, mass flux, and initial release time. The models included up to 25 unknown model parameters constrained by prior information and calibration data. Model analyses were particularly focused on exploring uncertainty in model parameters and conceptualizations. Various alternative conceptual scenarios were explored.

Retrospective examination of the published decision support analyses since 2008 related to source identification and monitoring network design demonstrates the accuracy of model predictions and the success of implemented decision-support techniques. The model analyses of the contaminant transport at the site provide important insights about the governing processes controlling future plume development and decision analyses related to potential future remedial activities.

The proposed methodology allows for efficient (1) evaluation of the uncertainty in model predictions (because of fast execution times); (2) estimation of 3D contaminant migration; (3) efficient estimation of plume dispersion; (4) estimation of the dimensions of the area associated with contaminant-arrival zones; (5) estimation of uncertainty in advective transport direction; (6) estimation of transients in contaminant transport; and (7) estimation of the impact of chromium reduction and retardation on contaminant transport using simple geochemical models. The methodology is general and the computational tools are flexible allowing for easy application at other contamination sites.

All the applied computational tools are embedded in the code MADS (http://mads.lanl.gov), which provides a computationally efficient and robust framework for various types of model analyses related to decision support; it also includes advanced novel techniques for decision analyses based on information gap theory [27]. This allows for computationally efficient, reproducible and defensible model-based analyses for decision support. Currently, MADS algorithms are also being implemented in a Decision Support Toolbox of ASCEM (*Advanced Subsurface Computing for Environmental Management*; http://ascemdoe.org) code development project funded by the U.S. *Department of Energy, Environmental Management*. ASCEM targets development of an interactive computer-based Decision Support System (DSS) that will help domain scientists, managers, regulators, and stakeholders make decisions related to site characterization, monitoring design, and remedial activities based on data- and model-driven decision-support analyses exploiting high-performance computing.

REFERENCES

1. Janssen, Ron, and Marjan van Herwijnen, (1992), *Multiobjective decision support for environmental management*. Dordrecht: Kluwer.
2. Walker, W. E., Harremoës, P., Rotmans, J., Van der Sluijs, J. P., Van Asselt, M. B. A., Janssen, P., & Von Krauss, M. K. (2003). *Defining uncertainty: a conceptual basis for uncertainty management in model-based decision support*. Integrated Assessment, 4(1), 5-17.
3. Matthies, M., Giupponi, C., & Ostendorf, B. (2007). Environmental decision support systems: Current issues, methods and tools. *Environmental Modelling & Software*, *22*(2), 123-127.
4. NMED/LANL Compliance Order on Consent, 2005, http://www.nmenv.state.nm.us/HWB/lanl/OrderConsent/03-01-05/Order_on_Consent_2-24-05.pdf
5. LANL, 2006. *Interim Measures Investigation Report for Chromium Contamination in Groundwater*, LA-UR-07-6018, Los Alamos, New Mexico.
6. LANL, 2008. *Fate and Transport Investigations Update for Chromium Contamination from Sandia Canyon*, LA-UR-08-4702, Los Alamos, New Mexico.
7. LANL, 2009. *Investigation Report for Sandia Canyon*, LA-UR-09-6450, Los Alamos, New Mexico.
8. LANL, 2012. *Phase II Investigation Report for Sandia Canyon*, LA-UR-12-24593, Los Alamos, New Mexico.
9. Stoker, A.K., 1977. *Tritium Measurements on Sewage Treatment Plant Effluents*, H8-77-242, Los Alamos, New Mexico.
10. Vesselinov, V.V., 2004, *An alternative conceptual model of groundwater flow and transport in saturated zone beneath the Pajarito Plateau*, LA-UR-05-6741, Los Alamos, New Mexico.
11. MADS, 2012, Integrated open-source computational framework for Model Analysis & Decision Support (MADS), http://mads.lanl.gov.
12. Wexler, E.J., 1992. *Analytical Solutions for One-, Two-, and Three-Dimensional Solute Transport in Ground-Water Systems with Uniform Flow*, Chapter B7 of *Techniques of Water-Resources Investigations of the United States Geological Survey*, United States Government Printing Office, Washington, D.C.
13. Park, E. , Zhan, H., 2001, *Analytical solutions of contaminant transport from finite one-, two-, and three-dimensional sources in a finite-thickness aquifer*, Journal of Contaminant Hydrology, 53, 41–61.
14. Wang, H., Wu, H., 2009, *Analytical solutions of three-dimensional contaminant transport in uniform flow field in porous media: A library*, J. of Frontiers of Env. Science & Engineering in China, 3, 112-128.
15. Domenico, P.A., 1987. An Analytical Model for Multidimensional Transport of a Decaying Contaminant Species, *Journal of Hydrology,* Vol. 91, pp. 49–58. (Domenico 1987)
16. West, M.R., B.H. Kueper, and M.J. Ungs, March–April 2007. On the Use and Error of Approximation in the Domenico (1987) Solution, *Ground Water,* Vol. 45, No. 2, pp. 126–135. (West et al. 2007, 106995)
17. Srinivasan, V., T.P. Clement, and K.K. Lee, March–April 2007. Domenico Solution—Is it Valid?, *Ground Water,* Vol. 45, No. 2, pp. 136–146. (Srinivasan et al. 2007, 106993)
18. Freeze, R.A., and J.A. Cherry, 1979. *Groundwater*, Prentice-Hall, Inc., Englewood Cliffs, New Jersey. (Freeze and Cherry 1979)
19. Gelhar, L.W., C. Welty, and K.R. Rehfeldt, 1992. A Critical Review of Data on Field-Scale Dispersion in Aquifers, *Water Resources Research,* Vol. 28, No. 7, pp. 1955–1974. (Gelhar et al. 1992).
20. Neuman, S.P., August 1990. *Universal Scaling of Hydraulic Conductivities and Dispersivities in Geologic Media*, *Water Resources Research,* Vol. 26, No. 8, pp. 1749-1758.
21. Levenberg, K. (1944). *A method for the solution of certain problems in least squares*. Quarterly of applied mathematics, 2, 164-168.
22. Marquardt, D. W. (1963). *An algorithm for least-squares estimation of nonlinear parameters*. Journal of the Society for Industrial & Applied Mathematics, 11(2), 431-441.
23. More, J. (1978). *The Levenberg-Marquardt algorithm: implementation and theory*. Numerical analysis, 105-116.
24. Vesselinov, V.V., D.H. Harp, *Adaptive hybrid optimization strategy for calibration and parameter estimation of physical process models*, Computers & Geosciences, doi: 10.1016/j.cageo.2012.05.027, 2012.
25. Harp, D., Vesselinov. V.V., *An agent-based approach to global uncertainty and sensitivity analysis, Computers & Geosciences, doi:10.1016/j.cageo.2011.06.025, 2011.*
26. Vesselinov, V.V., Harp, D., *Decision support based on uncertainty quantification of model predictions of contaminant transport*, CMWR 2010: XVIII International Conference on Water Resources, J. Carrera (Ed), CIMNE, Barcelona 2010.
27. Harp, D., Vesselinov. V.V., *Contaminant remediation decision analysis using information gap theory*, Stochastic Environmental Research and Risk Assessment (SERRA), DOI: 10.1007/s00477-012-0573-1, 2012.

ACKNOWLEDGEMENTS

This work was supported by the Los Alamos National Laboratory Environmental Programs Directorate (ADEP).